ratio on both facets is already known.

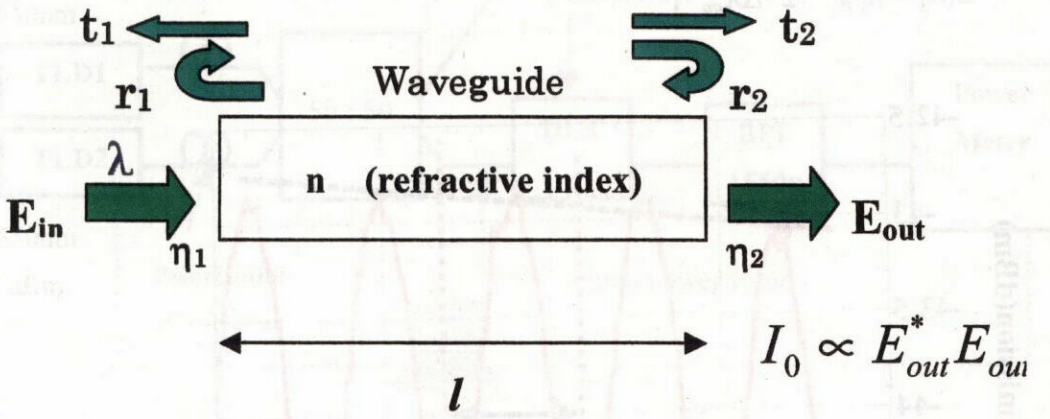

Fig.3.14. Schematic experimental setup for measuring waveguide propagation loss with Fabry-Perot method. t_1, t_2: transmission ratio. r_1, r_2: reflection ratio. η_1, η_2: coupling efficiency. E_{in}, E_{out}: input and output of electromagnetic filed of the lightwave. λ: wavelength. l: length of the waveguide. I_0: output intensity.

As shown schematically in Fig.3.14, with reflection ratio r_1 and r_2 at its two facets, the waveguide forms a Fabry-Perot etalon. When the light E_{in} couples into the waveguide, the power of the output light varies with the wavelength according to loop phase matching condition, as shown in formula (3.2). The loss of the waveguide then can be derived to (3.4), with the contrast H defined in (3.3).

$$I_0 \propto E^*_{out} E_{out} = \frac{\eta_1 \eta_2 t_1^{\,2} t_2^{\,2} e^{-\alpha l} |E_{in}|^2}{1 + r_1^{\,2} r_2^{\,2} e^{-2\alpha l} - 2 r_1 r_2 e^{-\alpha l} \cos(4\pi n l / \lambda)} \tag{3.2}$$

$$H \equiv \frac{I_{o\max}}{I_{o\min}} = \left(\frac{1 + r_1 r_2 e^{-\alpha l}}{1 - r_1 r_2 e^{-\alpha l}} \right)^2 \tag{3.3}$$

$$\alpha = -\frac{1}{l} \ln \left(\frac{1}{r_1 r_2} \cdot \frac{\sqrt{H} - 1}{\sqrt{H} + 1} \right) \tag{3.4}$$

Fig.3.15 gives an example of the measurement result by this method (#3534). We notice that the peak of the output oscillating in the form of $\cos(4\pi n l / \lambda)$. So from wavelengths of the adjacent two peaks, we can obtain

$$4\pi n l / \lambda_1 - 4\pi n l / \lambda_2 = 2\pi \tag{3.5}$$

So the refractive index of the waveguide can be obtained by

$$n = \frac{\lambda_2 \cdot \lambda_1}{2(\lambda_2 - \lambda_1)l} = \frac{\lambda_2 \cdot \lambda_1}{2 \cdot \Delta\lambda_{FP} \cdot l} \tag{3.6}$$

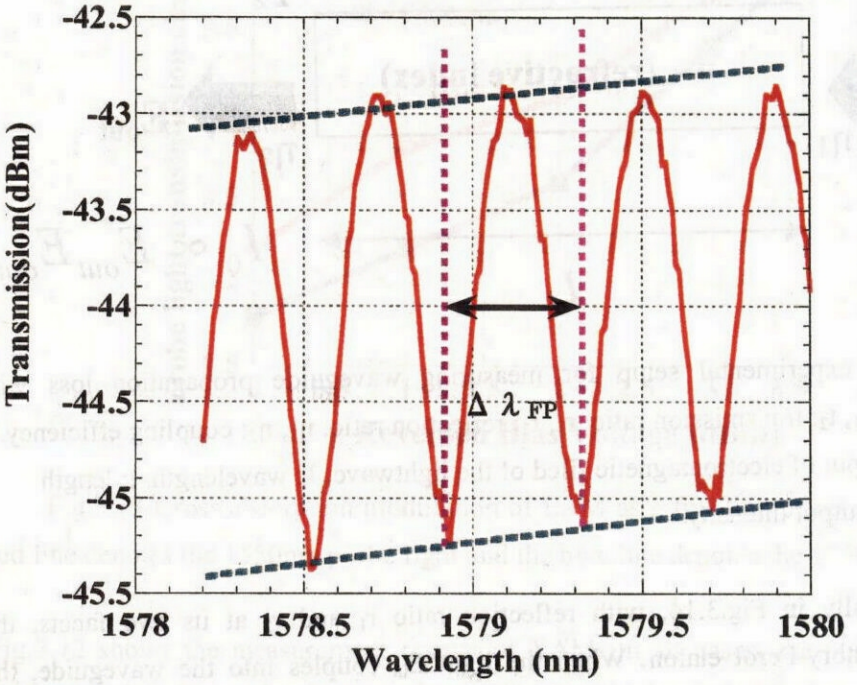

Fig.3.15 Fabry-Perot waveguide loss measurement result for sample #3534.

XPM

The phase shift in the waveguide can be expressed as

$$\Delta\phi = \frac{2\pi}{\lambda}(n' - n) \cdot l \tag{3.7}$$

Formula (3.7) denotes the phase change is always accompanied with the shift of the peaks. By measuring the refractive index repeatedly, we can finally obtain the phase shift.

Fig.3.16 shows the experimental setup for the measurement of XPM. The CW pump light is at 1530 nm, and the CW probe light varies form 1540nm to 1580nm with the power of 0dBm from the TLD2. The input power of the pump light after the 3dB coupler varies from -15dBm to 8dBm. The EAM is biased at 0V. Bandwidth of the BPF is 1 nm. The polarization controllers (PC1 and PC2) are used to set the outputs in TE modes for both probe and pump lights. The EAM is cooled at 20 °C.

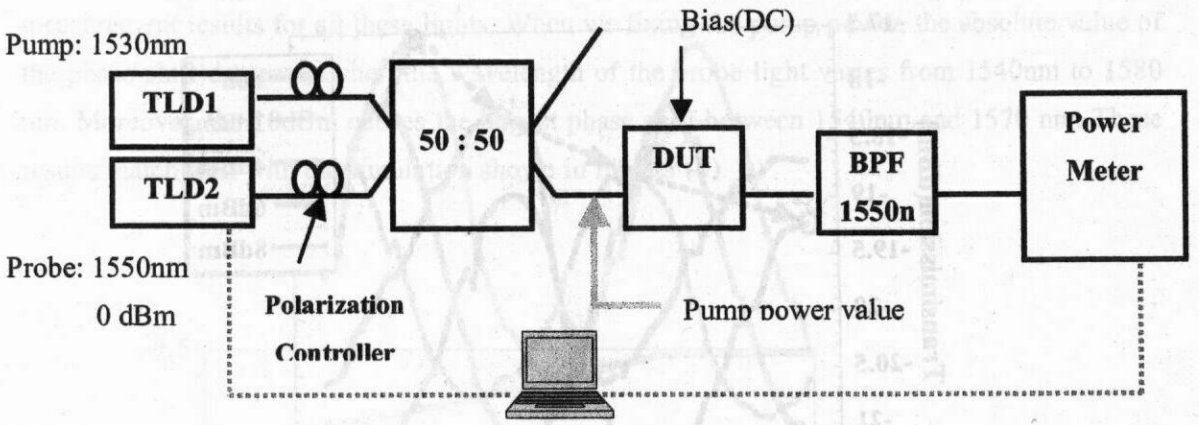

Fig.3.16 Experimental setup for the measurement of cross phase modulation. DUT: device under test.

Fig.3.17 shows the Fabry-Perot Etalon measurement results of EAM when the probe light is at 1550nm. As shown by the arrows that the peak shifts to the short wavelength while the input power of the pump light increases from on power to 8dBm.

Based on Fig.3.17, the phase shift can be calculated according to expression (3.7), and the results are shown in Fig.3.18. We see that the absolute value of the phase change increases with the pump power. π and 2π shifts are obtained at the power of 6.2dBm and 9.6dBm. Considering that in the above experiment, both the probe light and pump light are continuous waves, these two power values are not so large. That means in the EAM, the XPM is strong enough to be applied in really devices. Note that in Fig.3.18, the data is not depicted when the pump power is smaller than 2dBm.

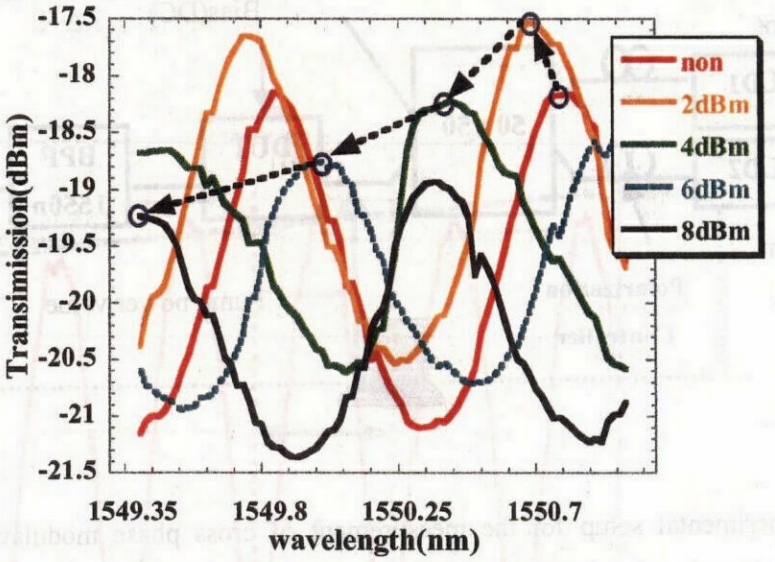

Fig.3.17 Fabry-Perot Etalon measurement result of EAM. The wavelengths of the pump light and probe light are 1530nm and 1550 respectively. The power of the probe light is 0dBm.

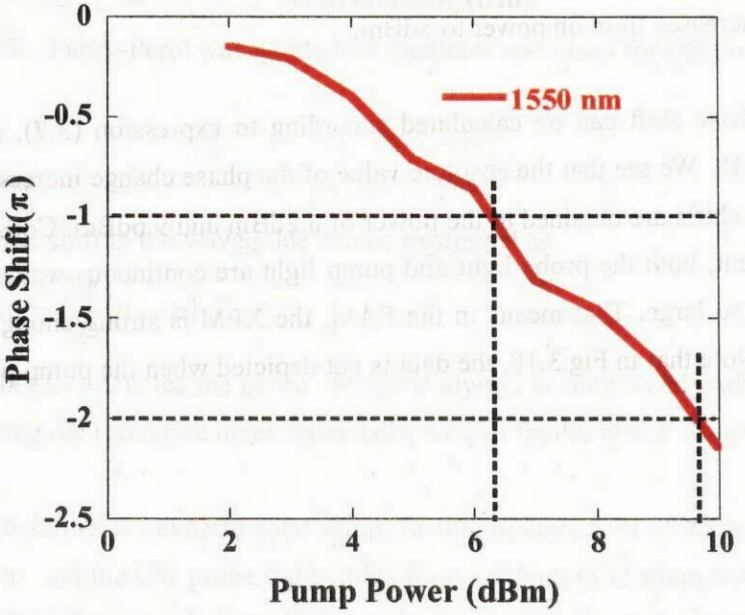

Fig.3.18 Phase shift result of EAM. The wavelengths of the pump light and probe light are 1530nm and 1550 respectively. The power of the probe light is 0dBm.

As mentioned before, we measured the XPM from 1540nm to 1580nm. Fig.3.19 gives the XPM measurement results for all these lights. When we fixing the pump power, the absolute value of the phase shift decreases when the wavelength of the probe light varies from 1540nm to 1580 nm. Moreover, the 10dBm causes the largest phase shift between 1540nm and 1570 nm. These results match well with the simulation shown in Fig.3.5 (b).

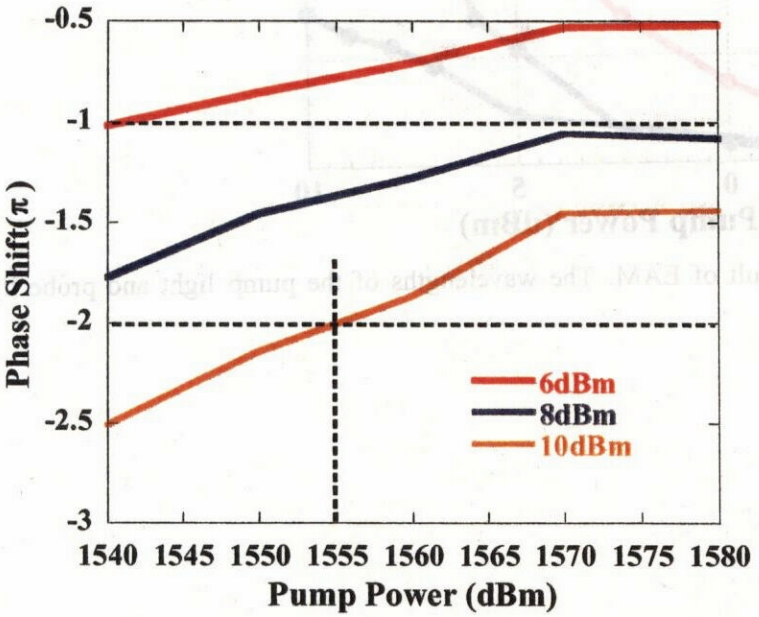

Fig.3.19 Phase shift result of EAM as function of the wavelength of the probe light. The wavelength and power of the pump light are 1530nm and 0dBm.

In my experiment, I fixed the bias at 0V. So the bias voltage's effect on the XPM was not measured. I cited the measurement results from Mr.Kaneko's master thesis [5] and show them in Fig.3.20. The y-axis denotes the absolute value of the phase shift. We can see, when the bias voltage varies from 0V to 2V, the absolute value of the phase shift decreases, which means the weakening of the XPM. We think this is because under high bias voltage, the photo-generated carriers by the pump light are dramatically swept out by large electrical fields, thus the pump light does not undergo much carrier density change which originates the XPM.

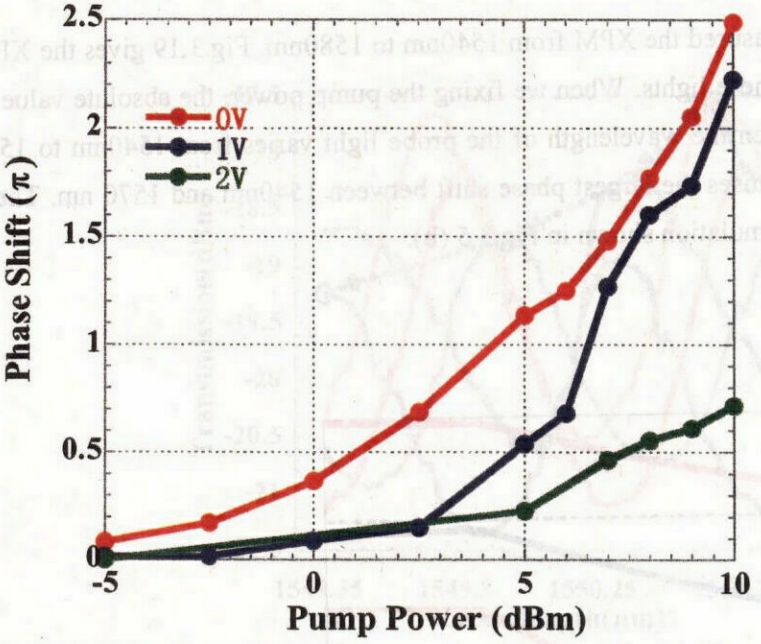

Fig.3.20. Phase shift result of EAM. The wavelengths of the pump light and probe light are 1530nm and 1570dBm.

3.4 Summary

The main target in this chapter is to investigate the nonlinearity in an EAM with InGaAlAs/InGaAlAs MQW. For this purpose, we firstly introduced the theoretic analysis of the QW structure. From the simulation, we saw that the change of the carrier density determines the changes of the absorption coefficient and the refractive index, which indicate the effects of XAM and XPM. Then the fabrication of the EAM with InGaAlAs/InGaAlAs MQW grown by MOVPE is introduced. In the third part, we showed the measurement results of a single EAM. Attention was focused to the measurement of the XAM and XPM. According to the results, both XAM and XPM were clearly observed. For XAM, the shorter the wavelength of the pump light is, the more the absorption coefficient changes; the intensity of the XAM also increases with the increase of the reverse bias voltages. XPM had the similar dependence on wavelength, however, it weakens when the bias voltage increases. In the fabricated EAM, 2π phase shift was obtained

when the input power was 9dBm including 7dB coupling loss. The measurement results match well with the simulation. In this way we have finished the basic work for the wavelength converter and all-optical switch in Chapter IV and V: the fabrication of the EAM and the confirmation of the nonlinearity in EAM.

References

[1] Masaki Kato, Ph.D thesis "正樹高性能電界吸収型光変調器のための InGaAs/InAlAs/InP 変調ポテンシャル量子井戸に関する研究", 2001

[2] G. D. Sanders and Y. C. Chang, ."Theory of photoabsorption in modulation-doped semiconductor quantum wells", Phys. Rev. B, vol. 35, pp. 1300-1315, 1987.

[3] G. D. Sanders and K. K. Bajaj, "Electronic properties and optical-absorption spectra of GaAs-AlxGa1-xAs quantum wells in externally applied electric fields", Phys. Rev. B, vol. 35, pp.2305-2320, 1987.

[4] G. Bastard, E. E. Mendez, L. L. Chang, and L. Esaki, "Variational calculations on a quantum well in an electric field", Phys. Rev. B, vol. 28, pp. 3241-3245, 1983.

[5] S.Kaneko, master thesis, "全光スイッチ/波長変換に向けた InGaAs/InAlAs 電界吸収型変調器における相互吸収変調/相互位相変調の測定", 2004.